Research Article Vol. 30, No. 4 / 14 Feb 2022 / Optics Express 6258
Optics EXPRESS

Assembly-level topology optimization and additive manufacturing of aluminum alloy primary mirrors

LEI YAN,[1] XIN ZHANG,[1,*] QIANG FU,[1] LINGJIE WANG,[1] GUANGWEI SHI,[1] SHUANGLONG TAN,[1,2] KAI ZHANG,[1,2] AND MINGXIN LIU[1]

[1] *Key Laboratory of Optical System Advanced Manufacturing Technology, Changchun Institute of Optics, Fine Mechanics and Physics, Chinese Academy of Sciences, Changchun, Jilin 130033, China*
[2] *University of Chinese Academy of Sciences, Beijing 100049, China*
[*] *optlab@ciomp.ac.cn*

Abstract: Additive manufacturing can realize complex structures that cannot be achieved by conventional manufacturing methods. At the same time, topology optimization provides more excellent solutions for structural design. In the field of guidance and navigation optics, ultra-lightweight, high rigidity, and high integration are important requirements. Metal mirrors are widely used in this field due to their good processing performance. In this paper, we describe the integrated design and manufacturing of aluminum alloy primary mirror assembly (mirrors and mirror backplane) through the combination of additive manufacturing technology and topology optimization. Compared with the conventional design, it shows better performance.

1. Introduction

In recent years, guidance and navigation optical systems have played an increasingly important role in military strategy. To increase the rapid response capability, the systems need high rigidity and high lightweight. As the most important part of the guiding and navigation optical system, the mirrors need to meet the above requirements. Metal mirrors, especially aluminum alloy mirrors, have many excellent properties, such as short processing time, low material cost, and good processing technology. They are widely used in this field [1–5].

The manufacturing methods of conventional aluminum alloy mirrors have certain limitations in terms of lightweight and specific mechanical properties. Additive manufacturing (AM) can effectively solve this problem and provide a new concept for aluminum alloy mirror manufacturing [6–8]. At the same time, topology optimization provides a new idea for mirror design from the perspective of design methods. For example, Park et al. proposed the topology optimization of multispectral mirrors under self-weight [9,10]. The optimized mirrors have good optomechanical performance. Liu et al., realized the design of large-aperture mirrors through topology optimization methods [11]. In addition, Liu et al. carried out a topology optimization design on the space mirror based on parameter optimization, which fully realized the improvement of lightweight rate, optical performance, and structural rigidity [12].

As mentioned above, there have been many outstanding research results. Furthermore, the combination of AM and topology optimization methods can realize the high optomechanical performance in the single mirror structure [8,13].

However, from a system-level consideration, how to ensure that the optimized optical structure still maintains high optical surface stability after the system assembly is critical. Taking the mirror as an example, the mounting flatness, mounting stress, and thermal mismatching due to material parameter differences, directly affect the accuracy and stability of the optical surface of the mirror, during the assembly of the mirror and backplane [14]. Even the insufficient releasing

#453585 https://doi.org/10.1364/OE.453585
Journal © 2022 Received 12 Jan 2022; revised 29 Jan 2022; accepted 30 Jan 2022; published 10 Feb 2022

Optics EXPRESS

of residual mounting stress can directly affect the system's service life of the system. This requires strict control of optical and structural assembly during the integration process.

If this issue is taken into consideration from the beginning of the design, the risk of system integration will be greatly reduced and the stability of the system will be improved. In this paper, by combining AM and topology optimization methods, the integrated design and manufacturing of the mirror and its backplane are realized, which effectively solves the above problems, and gives full play to the advantages of AM. Through theoretical calculations, the mirror support scheme and thickness were designed. And then, combine lattice filling and equivalent analysis methods to realize the passive integrated and athermal design for the mirror assembly (mirror and backplane), which was verified by analysis and testing.

2. Performance

Usually, the optical system is manufactured, assembled, and tested on the ground. Therefore, the system needs to withstand strong shock and vibration conditions during the launch phase. In this case, the mirror is required to have sufficient surface accuracy and dynamic stiffness. This paper takes the mirror assembly in the small catadioptric optical system as the research object. The diameter of the mirror is 58 mm. The performance indicators include the maximum weight of the assembly, the accuracy of the mirror surface under self-gravity and mounting flatness, and the surface deformation during polishing. Because this article adopts the integrated design of the mirror and the mirror backplane, it avoids the mounting sensitivity and the risk of external force introduction during the mounting process. Through the design requirements of the optical system, the system-level quantitative indicators are set. The requirements: 1) The area density of the mirror assembly is less than 20 kg/m^2, reaching the level of the mirror alone; 2) The surface shape of the mirror under the self-weight is less than RMS 3 nm, and under mounting flatness at 0.003 mm is less than RMS 5 nm; 3) The surface deflection (quilting) of the mirror aperture surface under polishing pressure is less than (peak to valley, PV) 43 nm.

3. Design of aluminum alloy major mirror assembly

In this section, an integrated design scheme of mirror assembly including multiple analysis methods is developed. The assembly structure is optimized and assembled on the external load transmission path to realize the ultra-lightweight design of each regional structure while ensuring the assembly-level performance meets the index requirements of Section 2.

For the aluminum alloy mirror assembly material used in this paper, the first to determine the mirror support plan, while introducing the mirror density and giving a reasonable initial value of the mirror thickness. Combined with the requirements of quilting, a lattice filling method based on a specific structure is adopted to implement the lightweight design of the mirror. Secondly, the equivalent analysis method is introduced, and the topology optimization design of the mirror support area is performed on the external load transmission path, generating a refined mirror assembly structure. Finally, through finite element analysis, the reasonableness of assembly design was verified. Figure 1 provides a flow chart of the integrated design scheme of the mirror assembly.

3.1. Mirror support plan and mirror thickness

The ways of mirror support can be classified as the central support, peripheral support, side support, and back support, according to the support position [15]. The selection of the support method is directly related to factors such as material, aperture, and weight. The central support is suitable for mirrors whose mass is concentrated in the center. The peripheral support is suitable for mirrors with low strict quality requirements and larger diameters. It has the characteristics of a simple support structure and a large support base. The side support is suitable for non-circular

Optics EXPRESS

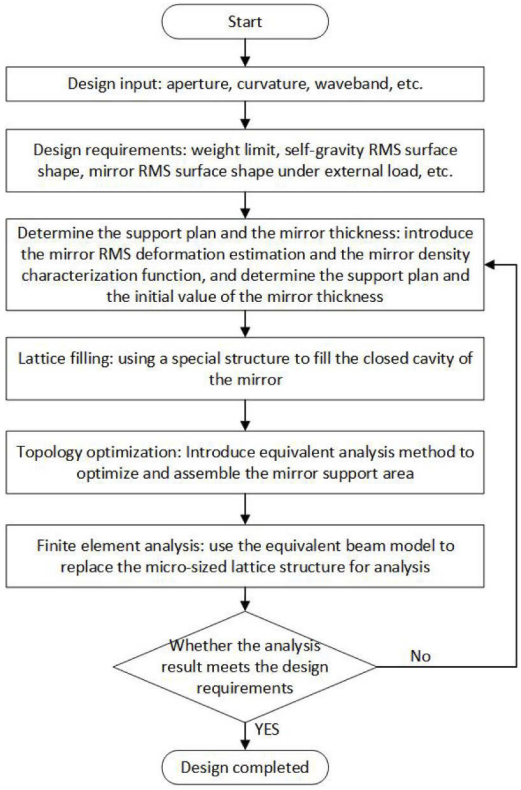

Fig. 1. Flow chart of integrated design scheme of the mirror assembly.

symmetrical mirrors, often used in long mirrors. The back support has no special requirements for the diameter of the mirrors and is usually suitable for mirror material structures with higher stiffness.

As mentioned above, when aluminum alloy materials are selected for the integrated design of mirror assembly, this paper focuses on the material properties, mirror aperture, and combines the high index requirements in Section 2 to determine the support scheme. Given the characteristics of the shape of the mirror, the peripheral and side support solutions are temporarily excluded here. According to the thin plate assumption, the RMS of the mirror surface can be analyzed and estimated by Eq. (1) [16].

$$\delta_{RMS} = C\frac{\rho g}{E}\frac{r^4}{{h_b}^2}(1-\nu^2) \tag{1}$$

where C is the constant of the mounting conditions, ρ is the material density, g is gravitational acceleration, r is the semi-diameter of the mirror, ν is Poisson's ratio, h_b is equivalent bending thickness. For open-back and closed-back mirrors, the equivalent bending thickness derivation can be obtained in the study of Mehta et al. [17]. For an open-back mirror, the equivalent thickness can be obtained from Eq. (2).

$$h_b = \left(\frac{(1-k\eta)({t_f}^4 - k\eta {h_c}^4) + k\eta(t_f + h_c)^4}{t_f + k\eta h_c}\right)^{\frac{1}{3}} \tag{2}$$

where k is the effectiveness factor of ribs, η is areal solidity ratio, t_f is face sheet thickness, h_c is the isogrid cell depth.

Optics EXPRESS

It can be seen that for the same mirror geometry, the surface shape of the mirror is directly proportional to the specific stiffness ($\frac{E}{\rho}$) of the material. Table 1 below lists several conventional mirror material parameter comparisons.

Table 1. Comparison of material parameters of conventional mirrors

Material	Density ρ/kg·m^{-3}	Young's modulus E/GPa	Thermal conductivity λ/W·mK^{-1}	Thermal expansivity α/K^{-1}
SiC	3200	400	155	2.4E-06
Si	2330	131	137	2.6E-06
Aluminum alloy	2700	68	167	23E-06

At the same time, for mirrors of the same quality, high surface quality can be achieved by adjusting the support position to coincide with the neutral surface. But it should be specially pointed out that under the condition of horizontal gravity (the optical axis is parallel to the direction of gravity), taking the uniformly distributed three-point support as an example, each support point needs to bear one-third of the mirror's weight. Near the support points of the mirror, the peak value of PV is linearly related to the elastic modulus of the mirror material, as shown in Fig. 2.

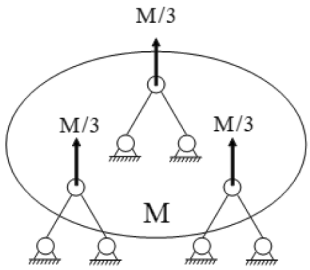

Fig. 2. Three-point support form of a mirror.

It can be seen that the feasibility of the back support scheme was studied by comparing the specific stiffness of the materials and combining the requirements for the elastic modulus of the materials under the horizontal working condition. Because of the research objects in this paper, it is less feasible to adopt a back support scheme similar to SiC mirrors. The central support scheme can fully meet the requirements for high integration and lightweight of the mirror in this paper. Furthermore, the transmission path of the external load to the mirror surface is lengthened, which is conducive to the stability of the mirror surface. After a comprehensive comparison, the central support scheme is selected.

In the selection of the thickness of the mirror surface, the thickness of the mirror needs to be controlled within a certain range to achieve a high light-weight rate. Generally, the mass per unit area of the mirror is used to measure the light-weight rate of the mirror, as shown in Eq. (3).

$$\frac{m}{A} = \rho(t_f + \eta h_c) \tag{3}$$

where, $\frac{m}{A}$ is areal mass density, ρ is the material density, η is the solidity ratio, h_c is the isogrid cell depth.

Calculating with the aluminum alloy material selected in this paper, the maximum mirror thickness of the mirror is about 7 mm under the requirement of 20 kg/m^2. However, in this case, η is approximately 0, and the lightweight rate of the mirror is extremely low. Therefore,

Optics EXPRESS

the surface shape is difficult to control at a better threshold level. Finally, the thickness of the primary mirror surface is selected as 2 mm, considering the requirements of subsequent optical processing, and the design parameters of the mirror in this paper.

3.2. Lattice filling

After theoretical calculations, the initial thickness of the mirror surface, which is limited by processing and manufacturing constraints, is given. Generally, conventional mirrors cannot be designed to be closed in structure. It is difficult to achieve the high rigidity of the mirror in the true sense and inevitably lose structural rigidity.

The use of AM methods effectively solves the above problems. Unlike conventional subtractive manufacturing, AM does not require a line of sight to create geometric shapes. Therefore, AM brings great freedom in design. Based on the initial thickness of the mirror, the initial closed cavity structure of the mirror is formed, and a specific form of lattice filling is carried out in the closed cavity to replace the conventional isogrid openback structure, which reduces the loss of system stiffness. Lattice filling allows small lattice cell size and mirror thickness, effectively reducing areal density. On this basis, for the high surface shape requirements, the mirror design needs to consider the surface shape change caused by the polishing pressure during the polishing process (called the quilting effect). Here, we can estimate by the unit size and unit geometry [18], as shown in Eq. (4).

$$\delta_q = \psi \frac{P}{E}\frac{B^4}{D} = 12\psi \frac{P}{E}\frac{B^4}{t_f{}^3}(1-\nu^2) \tag{4}$$

where, δ_q is the deflection over the unit cell, P is the polishing pressure, E is the modulus of elasticity, B is the inscribed cell diameter, D is the flexural rigidity, ψ is a cell geometry constant with the triangular cell. Note that the equation is independent of the depth of the cell. To quantify the effect from these localized surface deformations, Vukobratovic derives the Strehl ratio as a function of the wavelength and quilting deflection, as shown in Eq. (5).

$$S = \frac{I_i}{I_0} = \frac{4\pi^2\left(\frac{\delta_q}{2\lambda}\right)^2}{\left[1-2\pi^2\left(\frac{\delta_q}{2\lambda}\right)^2\right]\left[1-4\pi^2\left(\frac{\delta_q}{2\lambda}\right)^2\right]} \tag{5}$$

For a test wavelength of 632.8 nm and a Strehl ratio constraint of 0.95, this equates to a quilting deflection allowance of PV 43 nm. Compared with the calculated value of quilting theory under the conventional design form, complete the lattice selection and detailed design.

There are various forms of the lattice structure, such as the periodic structure of the honeycomb unit [6]. In this paper, the lattice is designed concerning the high stability of the space truss structure. The lattice structure is shown in Fig. 3.

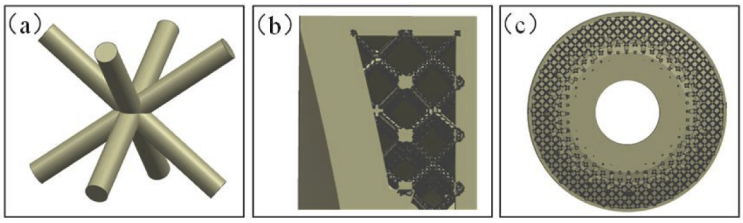

Fig. 3. Lattice structure. (a) lattice element, (b and c) sectional views of lattice arrangement in the closed cavity structure.

Optics EXPRESS

3.3. Equivalent analysis

Here, we can directly use the topology optimization method to complete the integrated structure design of the mirror assembly by taking the surface shape of the mirror as the optimization goal. Firstly, this method is feasible, but there are some problems: 1) Whether the thickness of the optimized mirror is reasonable or not, it needs further theoretical verification; 2) Because the surface shape is the result of multiple factors, the directly optimized structure cannot cover all working conditions, and it is generally the local optimal result under specific conditions; 3) Direct optimization is difficult to achieve a high lightweight rate index. For the mirror support area, it is difficult to achieve the same optimal design as the mirror surface shape.

Given the above problems, combined with the high stiffness, high lightweight rate, and high surface stability of the integrated design of the mirror assemble in this paper, a design idea based on the equivalent analysis method is proposed. It is shown in Fig. 4. First, based on the foregoing theoretical calculations, the mirror support scheme is selected. In addition, the initial thickness of the mirror surface and the lattice form of the closed structure on the back of the mirror is given. meanwhile, the theoretical estimation of the mirror surface accuracy and the quilting effect is completed. Then, starting with the force transmission path from the external load to the mirror surface and isolating the mirror assembly, meanwhile, making the mirror base (the mirror surface and the closed structure on the back of the mirror surface) equivalent to a rigid mass point, which is loaded on the supporting structure of the mirror through a load form. setting the external constraint boundary conditions, and using the mirror support structure as the design area for topology optimization design to achieve the high mechanical performance of the mirror support area while ensuring the stability of surface accuracy.

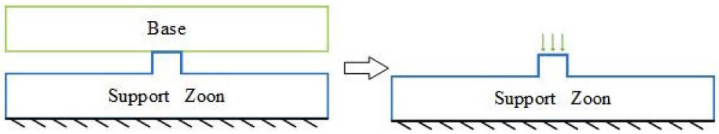

Fig. 4. Equivalent analysis and design ideas of the mirror assembly.

3.4. Optimal design

Based on the equivalent analysis model, the topological optimization design of the support structure is first developed. Through the analysis of the force transmission path, the optimal material distribution is found in the design space, to achieve the design purpose of high stiffness and high lightweight in the support area.

According to the common standards for surface shape evaluation, surface shape accuracy is the intuitive embodiment of the mirror position change. From the energy conservation, the strain energy of systems and external force work is transformed mutually, which follows the principle of minimum potential energy. Thus, the strain energy equation characterized by stiffness matrix and node displacement can be derived. In conclusion, the surface shape can be measured by the deformation of the internal unit, so the strain energy can be used to limit the surface shape. At the same time, high stiffness design is necessary to make the mirror assembly have high surface accuracy.

Optics EXPRESS

Taking volume as the constraint condition and minimum strain energy as the design goal, establish a mathematical optimization model, as shown in Formula (6).

$$\min : J(\alpha) = U^T KUi$$
$$s.t. \begin{cases} KU = F \\ V(\alpha) = fV_0 \\ 0 \le \alpha_i \le 1 \end{cases} \tag{6}$$

where J is the strain energy of the mirror support area, α is the design variable vector, α_i is ith design variable, K is global stiffness matrix, U is the global displacement vector, F is global load vector, V is the design domain volume constraints, f is volume fraction, and V_0 is design domain volume.

The variable density method is adopted, and the relative density of each element is taken as the design variable. On the non-critical path, the relative density is close to 0. Firstly, the constraints and loads are set according to the actual use. After the mirror base is equivalent, it is applied to the support area structure in the form of a load to establish an equivalent analysis model of the support area to be optimized (Fig. 5). The structural weight of the support area before the optimization is 26.1 g.

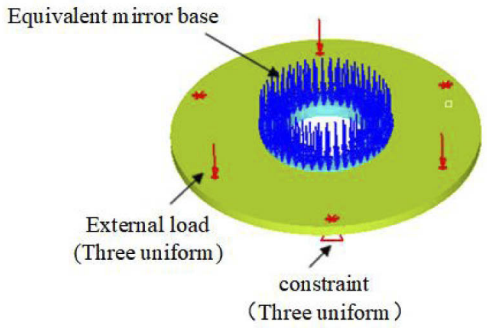

Fig. 5. The initial equivalent analysis model before optimization.

After 33 iterations, the result converges to a stable value. Then, the structural forms under different density thresholds are obtained by adjusting the density threshold. Figure 6 shows the structure form under different thresholds after 33 iterations of convergence. Red represents the main bearing area whose relative density is close to 1. Combined with the requirements of additive manufacturing, the optimization result at the 0.51 threshold level is selected as the final topology optimization result. The total weight of the optimized support area is 13.3 g.

Through topology optimization design, the optimal structure distribution of the mirror support area is realized. Similarly, from the optimization results, it can be seen that there is still space for further lightweight design without destroying the mechanical properties of the structure. Here, we formed a structural model of refined mirror support region based on the topology optimization results. On this basis, we further carried out a lightweight skeleton design for the main bearing region. And this area is further subdivided. Figure 7 shows the division of each region.

Referring to the excellent stability characteristics of the triangular beam, the load-bearing area 1 is layered and lightweight. And the overlapping design between layers ensures that the original design stiffness is not lost. The bearing area 2 and bearing area 3 can be properly hollowed out, and the supporting beam can be added at the position with the maximum bending moment. The lightweight process and the lightweight structure are shown in Fig. 8 and Fig. 9. After the

Optics EXPRESS

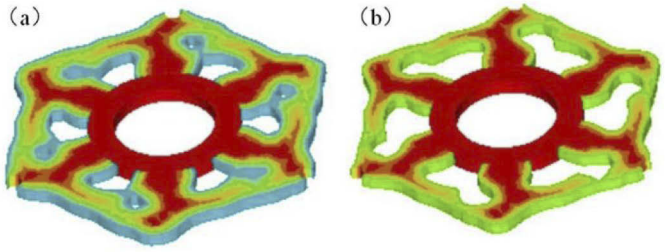

Fig. 6. (a) After 33 iterations, optimization results at different threshold levels. The structural form at the 0.2 threshold level, (b) the structural form at the 0.51 threshold level.

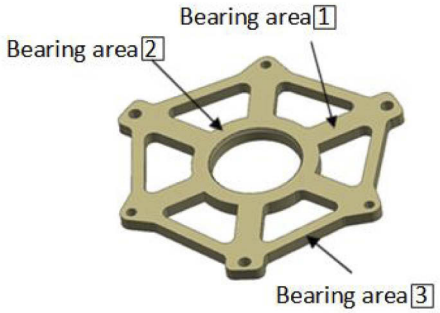

Fig. 7. Division of bearing area.

load-bearing area is lightened, the structural weight of the mirror support area becomes 12.1 g. The weight is reduced by 9% compared with the load-bearing area, and 53.6% compared with that before topology optimization.

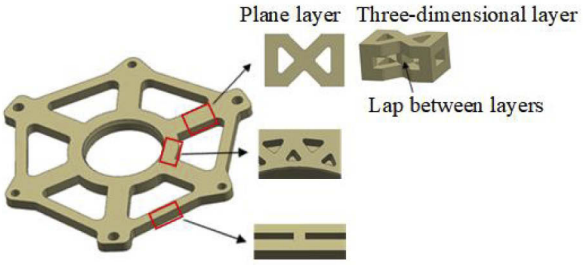

Fig. 8. The lightweight design process of the load-bearing area.

After topology optimization design, the entire mirror support area has achieved an ultra-light and high-rigidity design. Combining the aforementioned theoretical calculations, the entire mirror assembly design is completed through system assembly. Through system assembly, the entire mirror assembly design is completed. The structure of the mirror assembly is shown in Fig. 10. The final weight of mirror assembly is 36.3 g and the area density is 13.7 kg/m^2.

Optics EXPRESS

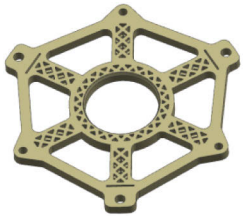

Fig. 9. Lightweight results of the mirror support area.

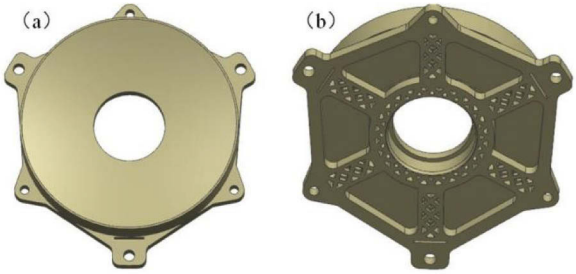

Fig. 10. (a) front view of the mirror assembly, (b) rear view of the mirror assembly.

4. Finite element analysis

Through Section 3, the structure design of the mirror assembly is completed. Here, the finite element analysis will be performed on the mirror assembly to obtain relevant indicators and verify the rationality.

Due to the use of a large number of micro-sized lattice structures, the operation time mainly depends on the minimum element size in the finite element analysis process. For this kind of micro-size, a fine element is required to avoid losing the characteristics of the structure itself. But this can inevitably increase the time for pre-processing and solving. To improve the efficiency and ensure the accuracy of analysis, it is necessary to carry out equivalent modeling of the lattice structure [8].

In view of the lattice structure adopted in this paper, a beam structure equivalent to replacing the complex lattice structure is provided. In the actual force state of the lattice, the force on the convergent point of the lattice structure is like the plastic hinge structure. Different from the structural hinge structure, it will bear the bending moment transmitted by each beam element at the convergence point. Therefore, the equivalent modeling process shown in Fig. 11 is adopted to simulate the force and deformation of the lattice structure.

According to the relevant indicators in Section 2, using the lattice equivalent model, the following will analyze the self-gravity surface shape, installation flatness, modal, and quilting effect of the optimized mirror assembly by equivalent analytical method.

4.1. Surface shape accuracy analysis

To make the mirror surface shape accuracy meet the system requirements, it is necessary to ensure that the mirror assembly has a high static surface shape. Here, the mirror assembly is first loaded with 1 g gravity to investigate the surface accuracy of the mirror assembly in three directions (an axial direction and two radial directions). At the same time, at the position of the external connection hole of the mirror assembly, by applying a forced displacement, the surface shape accuracy change of the mirror assembly due to the flatness of the installation is simulated.

Optics EXPRESS

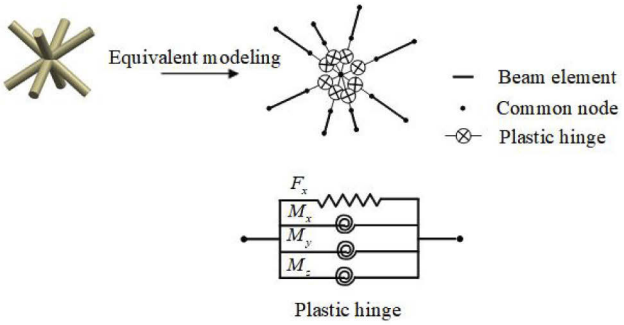

Fig. 11. Equivalent analysis model of the lattice structure.

By extracting the displacement of each point of the mirror surface shape, the surface shape fitting is carried out according to the theoretical optical curvature parameters. Figure 12 below shows the fitting result of the mirror surface under 1 g gravity.

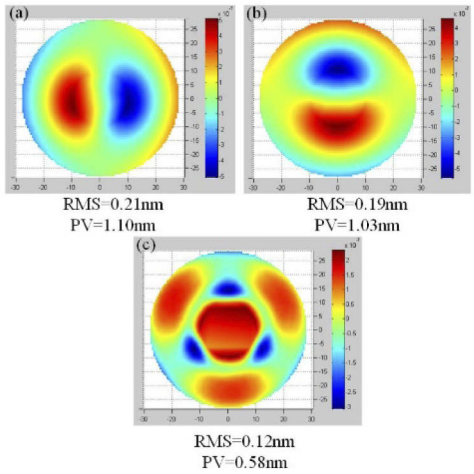

Fig. 12. The fitting result of the mirror surface is under 1g gravity of the mirror assembly. (a) Radial (x-direction) surface accuracy, (b) radial (y-direction) surface accuracy, (c) axial (z-direction) surface accuracy.

A 0.003 mm displacement is applied to the position of the mounting hole to simulate the effect of flatness on the surface shape of the mirror. Figure 13 below shows the accuracy of the mirror assembly under the influence of flatness alone.

The maximum surface shape of the mirror assembly under its gravity is RMS 0.21 nm, and the maximum peak value is PV 1.10 nm. For the external installation of the mirror assembly, at a mounting flatness level of 0.003 mm, the surface shape is RMS 4.7 nm and the peak value of PV is 18.6 nm. It can be seen from the above results that the optimized mirror assembly has sufficient surface accuracy in design and fully meets the index requirements of Section 2.

Furthermore, the bolt preload was analyzed to illustrate the sensitivity of the mirror surface shape to it. In terms of bolt size selection, combined with the mirror size and bolt locking requirements, M2 bolts which are made of stainless steel are finally determined at the mounting holes. The thread resistance torque of the thread pair and the friction torque between the bolts head and the supporting surfaces of the connectors must be overcome, during tightening the bolts.

Optics EXPRESS

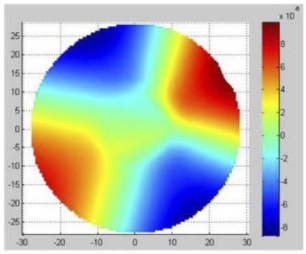

Fig. 13. Fitting results of mirror surface under 0.003 mm installation flatness.

Therefore, the installation torque was set at 0.2 N·m through certain theoretical calculations and experience. After determining these conditions, the separate preload simulation for the mirror assembly is carried out. The simulation analysis results are shown in Fig. 14, and the RMS surface shape changed by 1.37 nm. The results show that the surface shape has a low sensitivity to the bolt preload, and further reflects the advantages of integrated design.

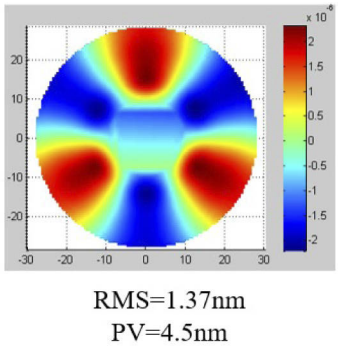

Fig. 14. Fitting results of mirror surface under the bolt preload.

4.2. Modal analysis

The optimized mirror assembly has a high lightweight rate. Further modal analysis is required to verify the sufficient local and overall stiffness of the optimized structure. Figure 15 shows the first three modes of the assembly, and Table 2 shows the mode participation factors ratios in each mode.

Table 2. Mode participation factors ratios in the first three modes

Order Direction	First-order mode	Second-order mode	Third-order mode
Translation in X	0.00458	0.61830	1.00000
Translation in Y	0.01466	1.00000	0.62420
Translation in Z	1.00000	0.00886	0.00896
Rotation around X	0.01432	1.00000	0.61840
Rotation around Y	0.00335	0.61920	1.00000
Rotation around Z	0.00011	0.00046	0.00078

Optics EXPRESS

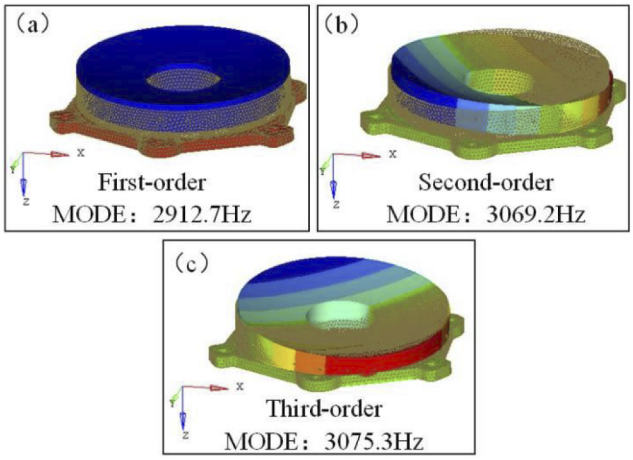

Fig. 15. Modal analysis results. (a) first-order mode, (b) second-order mode, (c) third-order mode.

It can be seen from the analysis results that the first-order mode of the mirror assembly is an axial translation mode, the second-order and third-order modes are rotation modes around the Y-axis and the X-axis, respectively. The first-order frequency of the mirror assembly is 2912.7 Hz.

4.3. Quilting analysis

It can be seen from Section 2 that the conventional backside grid structure will bring about PV 43 nm quilting deflection. For the lattice structure used in this paper, the quilting effect is mainly related to the mirror thickness and lattice structure. In areas far away from the mirror surface, the lattice structure contributes little to the quilting. We compared the hardness and specific stiffness characteristics of aluminum alloy and SiC. And combined with our experience, it is reasonable to select the polishing requirement of 10 kPa as the load condition in this paper, compared with that of SiC at 42kPa polishing pressure [17]. Figure 16 below shows the fitting result of the mirror surface quilting deflection under polishing pressure.

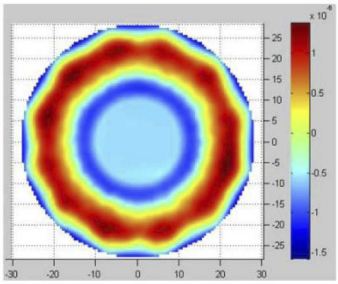

Fig. 16. Fitting result of the mirror surface PV quilting deflection under polishing pressure.

It can be seen that the surface shape is relatively uniform. The lattice structure effectively compensates for the mirror surface stiffness in the mirror substrate cavity, meanwhile. This also

Optics EXPRESS

confirms that the structure further from the facesheet has a negligible effect on surface quilting. Finally, the analysis results that quilting deflection under polishing pressure is PV 3.01nm.

5. Surface shape detection

Above, the final design and simulation analysis and verification of the mirror assembly have been completed. Here, we used a 3D printer to fabricate the assembly. After hot isostatic pressing (HIP) and stress relief treatment, a denser mirror assembly structure was obtained.

In the HIP, the mirror assembly is put into a closed container filled with inert gas. At the same time, the plastic deformation and densification of the material occur, under the action of high temperature (usually close to the forging temperature of the material) and high pressure (usually 100 to 140 MPa). The material isotropic property is also effectively improved. Moreover, the residual stress of the mirror assembly is relaxed to ensure the stability of the surface shape after the high-temperature annealing process under vacuum (high temperature 250 °C, heat preservation for 2 hours, natural cooling).

Finally, it was finished through post-stage optical processing, coating, and testing. Figure 17 below shows the results of the mirror surface after single point diamond turning (SPDT), coating and test (testing after assembling).

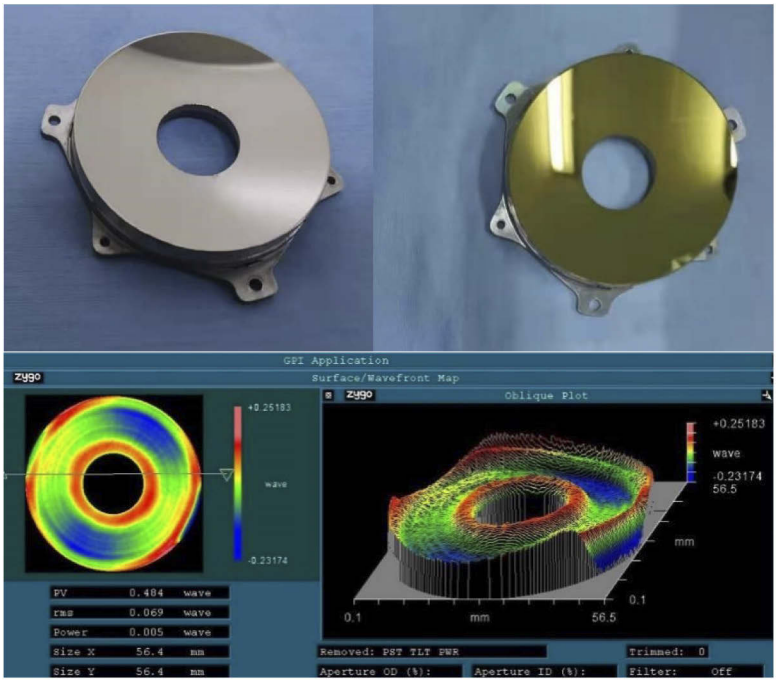

Fig. 17. Mirrors assembly after SPDT, coating, and optical inspection results of the mirror assemblies.

In order to obtain better surface quality, the surface is deposited with a NiP layer before SPDT. At the same time, the surface of the mirror was plated with gold to obtain high reflectivity.

Before assembling, we carried out further verification for the surface shape to examined the error between the detection results in the practical condition (both flatness and preload exist) and the simulation results. The workpiece setup is designed to simulate the installation state, and the surface shape is detected by LUPHOScan 260. Figure 18 shows the verification of workpiece setup and surface shape testing process.

Optics EXPRESS

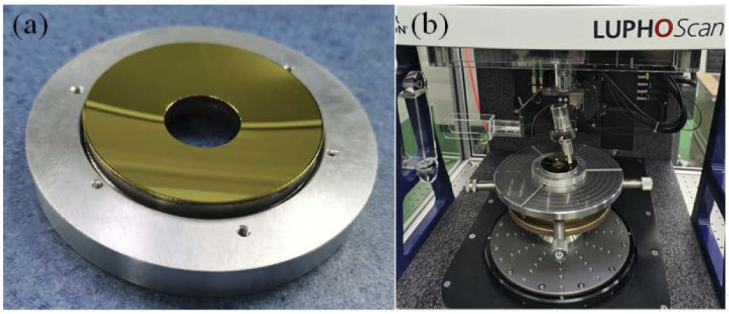

Fig. 18. (a) The mirror assembly is installed in the workpiece setup, (b) surface shape testing by LUPHOScan 260.

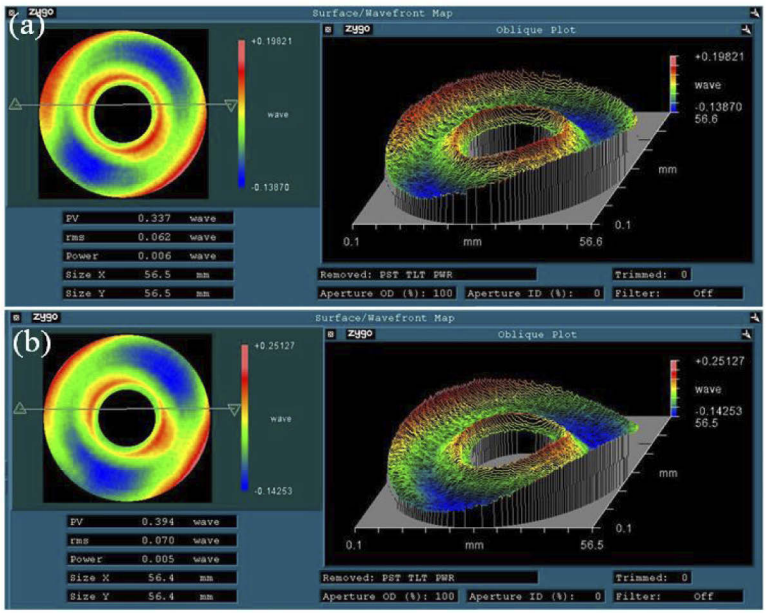

Fig. 19. (a) surface shape results of the mirror assembly under free state, (b) surface shape results of the mirror assembly under the bolt preload.

The connecting surface of the workpiece setup is processed by SPDT to ensure the validity and rationality of the error verification. Its flatness is approximately optical level (less than 0.5 μm). In addition, the installation flatness of the mirror assembly is realized by grinding, and the flatness is 0.003 mm, which ensures that the practical installation flatness is consistent with the simulation condition. And the same torque value as the simulation analysis is used to install the mirror assembly with fixed torque. Figure 19 shows the surface shape of the mirror assembly under free state and the bolt preload state.

The results show the surface shape of the mirror changes from the original RMS 0.062 λ (λ= 632.8 nm) to 0.070 λ (λ= 632.8 nm) after applying torque. According to the simulation analysis results of flatness and the bolt preload in Section 4.2, the simulation results of 0.003 mm flatness and 0.2 N·m preload are RMS 4.7 nm and RMS 1.37 nm, separately. It can be seen that the consistency between test and simulation analysis through data comparison.

Optics EXPRESS

It should be emphasized here that due to the tight project cycle, the mirror surface shape is only processed to the wavelength of RMS 0.069λ (λ=632.8 nm). The mirror surface has good stability during processing.

6. Conclusion

Here, combined with AM and topology optimization methods, we proposed the integrated design idea for aluminum alloy mirrors assembly and established a workflow. First, the mirror support scheme and mirror thickness are determined, through theoretical calculations. And the specific lattice structure is used to realize the closed design of the mirror base. At the same time, the quilting effect of the conventional mirror structure is estimated. Furthermore, the equivalent analysis method is introduced on the force transmission path, and the topological optimization design of the mirror support area is carried out. Among them, a large number of beam structures are used to make the lightweight design for the skeleton structure. Finally, the optimized mirror assembly was verified by finite element analysis. And the idea of equivalent modeling was adopted to provide a beam structure equivalent to replace the complex lattice structure for analysis and verification, which effectively improves the analysis efficiency and reduces the difficulty of pre-processing.

The mirror assembly designed in this paper achieves an areal density of 13.7 kg/m^2, and the surface shape of the mirror assembly under its weight is less than RMS 1nm. The surface shape of the mirror assembly under 0.003 mm mounting flatness is less than RMS 5 nm, and the fundamental frequency of the entire mirror assembly is greater than 2000 Hz. The mirror surface quilting deflection is PV 3.01 nm under polishing pressure, compared with the conventional isogrid design. The overall quilting deflection is reduced by 93%. Therefore, all analysis results meet the indicator requirements of Section 2.

This paper focuses on the integrated optimization design of the mirror assembly. In the future, further research will be carried out on the AM process of aluminum alloy mirrors and the stability of the optical and mechanical properties of the printed products.

Funding. National Natural Science Foundation of China (62005271).

Disclosures. The authors declare no conflict of interest.

Data availability. Data underlying the results presented in this paper are not publicly available at this time but maybe obtained from the authors upon reasonable request.

References

1. R. Steinkopf, A. Gebhardt, S. Scheiding, M. Rohde, O. Stenzel, S. Gliech, V. Giggel, H. Löscher, G. Ullrich, P. Rucks, A. Duparre, S. Risse, R. Eberhardt, and A. Tünnermann, "Metal mirrors with excellent figure and roughness," *Optical Systems Design* (SPIE, 2008), Vol. 7102.
2. S. Risse, A. Gebhardt, C. Damm, T. Peschel, W. Stöckl, T. Feigl, S. Kirschstein, R. Eberhardt, N. Kaiser, and A. Tünnermann, "Novel TMA telescope based on ultra precise metal mirrors," in *SPIE Astronomical Telescopes + Instrumentation* (SPIE, 2008), Vol. 7010.
3. H. P. Stahl, "Development of lightweight mirror technology for the next generation space telescope," in *International Symposium on Optical Science and Technology* (SPIE, 2001), Vol. 4451.
4. M. Y. Chen, L. Matson, H. Lee, and C. Chen, "Replication of lightweight mirrors," in *SPIE Optical Engineering + Applications* (SPIE, 2009), Vol. 7425.
5. L. Matson and M. Chen, "Enabling materials and processes for large aerospace mirrors," in *SPIE Astronomical Telescopes + Instrumentation* (SPIE, 2008), Vol. 7018.
6. E. Hilpert, J. Hartung, S. Risse, R. Eberhardt, and A. Tünnermann, "Precision manufacturing of a lightweight mirror body made by selective laser melting," Precis. Eng. **53**, 310–317 (2018).
7. H. Herzog, J. Segal, J. Smith, R. Bates, J. Calis, A. De La Torre, D. W. Kim, J. Mici, J. Mireles, D. Stubbs, and R. Wicker, "Optical fabrication of lightweighted 3D printed mirrors," in *SPIE Optical Engineering + Applications* (SPIE, 2015), Vol. 9573.
8. J. Mici, B. Rothenberg, E. Brisson, S. Wicks, and D. Stubbs, "Optomechanical performance of 3D-printed mirrors with embedded cooling channels and substructures," in *SPIE Optical Engineering + Applications* (SPIE, 2015), Vol. 9573.

Optics EXPRESS

9. K. S. Park, S. Y. Chang, and S. K. Youn, "Topology optimization of the primary mirror of a multi-spectral camera," Struct. Multidiscip. Optim. **25**(1), 46–53 (2003).
10. K.-S. Park, J. H. Lee, and S.-K. Youn, "Lightweight mirror design method using topology optimization," Opt. Eng. **44**(5), 053002 (2005).
11. S. Liu, R. Hu, Q. Li, P. Zhou, Z. Dong, and R. Kang, "Topology optimization-based lightweight primary mirror design of a large-aperture space telescope," Appl. Opt. **53**(35), 8318–8325 (2014).
12. G. Liu, L. Guo, X. Wang, and Q. Wu, "Topology and parametric optimization based lightweight design of a space reflective mirror," Opt. Eng. **57**(07), 1 (2018).
13. P. Jiang and P. Zhou, "Optimization of a lightweight mirror with reduced sensitivity to the mount location," Appl. Opt. **59**(12), 3799–3805 (2020).
14. J. H. Dong, "Ball Hinge Support Design and Analysis for Large Aperture Optical Mirror," OME Information (2010).
15. N. Horvath and M. Davies, "Advancing lightweight mirror design: A paradigm shift in mirror preforms by utilizing design for additive manufacturing," Appl. Opt. **60**, 3 (2020).
16. P. Mehta, "Flexural Rigidity Characteristics of Light-Weighted Mirrors," in *OE LASE'87 and EO Imaging Symposium* (SPIE, 1987), Vol. 0748.
17. E. Hilpert, J. Hartung, H. von Lukowicz, T. Herffurth, and N. Heidler, "Design, additive manufacturing, processing, and characterization of metal mirror made of aluminum silicon alloy for space applications," Opt. Eng. **58**(09), 1 (2019).
18. W. P. Barnes, "Optimal Design of Cored Mirror Structures," Appl. Opt. **8**(6), 1191–1196 (1969).